

Mid-infrared imaging of brown dwarfs in binary systems [★]

K. Geißler^{1,2}, G. Chauvin^{1,3}, and M. F. Sterzik¹

¹ European Southern Observatory, Alonso de Cordova 3107, Vitacura, Santiago, Chile
e-mail: kgeissle@eso.org, gchauvin@eso.org, msterzik@eso.org

² Max-Planck-Institut für Astronomie, Königstuhl 17, D-69117 Heidelberg, Germany

³ Laboratoire d'Astrophysique, Observatoire de Grenoble, UJF, CNRS; BP 53, F-38041 GRENOBLE Cedex 9 (France)

Received [date]; accepted [date]

ABSTRACT

Context. Brown dwarfs exhibit complex atmospheric signatures, and their properties depend sensitively on effective temperature, surface gravity, and metallicity. Several physical properties of brown dwarfs in binary systems can be well inferred from the primary, and therefore allow to better constrain their atmospheres.

Aims. We want to constrain atmospheric models of brown dwarfs in binary systems using narrow-band mid-infrared photometry.

Methods. High spatial resolution and sensitivity is required to resolve the components. Therefore we have obtained deep mid-infrared images of four close binary systems with brown dwarf companions using VISIR at the VLT in three narrow-band filters at 8.6, 10.5 and 11.25 μm .

Results. Three brown dwarf companions (GJ 229 B, HD 130948 BC and HR 7329 B) were detected at 8.6 μm . HD 130948 BC was also observed at 10.5 μm . We finally place upper flux limits for the other narrow band filters with null detections.

Conclusions. Our results are in general compatible with previous observations and model expectations for these objects. For HD 130948 BC, we conclude photometric variability on a significance level of 2.8σ based on repeated observations. The bandpass around 10.5 μm appears specifically well suited for variability studies, and we speculate that either inhomogeneities in the atmospheric NH_3 distribution, or silicate absorption might cause its time-variability.

Key words. Stars: low-mass, brown dwarfs – Stars: fundamental parameters

1. Introduction

Brown dwarfs (BDs) bridge the gap in mass between low-mass stars and giant planets. Hundreds of them have been discovered in the past decade, mainly in wide-field optical (SDSS, Stoughton et al., 2002) and near-infrared (e.g., 2MASS, DENIS; Cutri et al, 2003, Epchtein et al, 1997) surveys. Two main classes of BDs emerged from their optical and infrared spectral properties, the L-dwarfs and T-dwarfs. They typically cover effective temperature ranges of $T_{\text{eff}} \approx 2200 - 1400$ K and $T_{\text{eff}} \approx 1400 - 700$ K respectively. The modelisation of atmospheres cooler than $T_{\text{eff}} \leq 2000$ K is a challenge, because it must include an appropriate treatment of a plethora of molecular opacity's and dust processes (formation, condensation, size distribution and mixing). The most recent atmosphere models are including additional properties such as age (gravity) and metallicity and seem to reproduce reasonably well the spectral signatures and the infrared colors of L and T dwarfs. Only the L-T transition, occurring around a relative narrow temperature range $T_{\text{eff}} \approx 1300 - 1400$ K, remains problematic (for a discussion of state-of-the-art models see Burrows et al., 2006).

As an additional complication, the determination of distances, ages and metallicity for field BDs remains difficult and may be the cause of various uncertainties of their physical parameters. In that sense, BD companions of nearby stars are extremely interesting as the system characteristics are well known thanks to the

bright primary star. For these systems the influence of age and metallicity on the spectral signatures of substellar objects can be explored with high accuracy.

Initially, most BD studies were conducted in the optical and near-infrared. However, with the recent development of mid-infrared observing techniques and instruments from the ground or from space, this spectral region became essential as numerous molecular lines, including dominant absorption bands of CH_4 , CO , H_2O and NH_3 , are present. The *Spitzer Space Telescope* has provided a wealth of high-quality photometry and low- and medium resolution spectroscopy of L and T dwarfs in the $5 - 20 \mu\text{m}$ regime (see, e.g. Leggett et al., 2007; Cushing et al., 2006; Mainzer et al., 2007). They enable to probe, vertical mixing, clouds and non-equilibrium chemistry around the L – T boundary in unprecedented detail.

The power of sensitive, ground-based high spatial resolution mid-infrared imaging has recently been demonstrated for the close BD binary companion ϵ Indi Ba and Bb (see Sterzik et al., 2005). The *relative photometry* between both components allows to derive effective temperatures, independently from the determinations in near-infrared. As the distance is well known with the primary, the *absolute photometry* constrains radii and bolometric corrections, in contrast to *Spitzer* observations (Roellig et al., 2004) that suffered from insufficient angular resolution to resolve both components (*Spitzer* diffraction limit at $10 \mu\text{m}$ is $\sim 3''$).

In order to continue our effort to constrain atmospheric and evolutionary models of BDs, we have therefore conceived a

[★] Based on observations made with ESO Telescopes at the Paranal Observatories under programme ID's 076.C-0556(A) and 077.C-0438(A).

Table 1. Target Properties.

Object	π [mas]	Age [Gyr]	[M/H]	separ. [arcsec]	P.A. [degree]	Spectral type B	T_{eff} [K]	log g
GJ 229 (1)	173.19	0.2 (1) 0.030 (2)	-0.1 - -0.5 (4) -0.5 (2)	7.761 ± 0.007 (3)	163.5 ± 0.1	T6.5	950 ± 80 (4) 1000 ± 100 (2)	5 ± 0.5 (4) ≤ 3.5 (2)
HD 130948 (5)	55.73	0.3 - 0.8 (6-8)	0.0 (10)	2.64 ± 0.01 (5)	104.5 ± 0.5	L4 \pm 1* (10)	1900 ± 75 (9)	
HR 7329 (11)	20.98	0.012 (12)		4.17 ± 0.05 (11)	166.8 ± 0.2	M7/M8 (11)	2600 ± 200 (11)	
HR 7672 (13)	56.60	1. - 3. (13)	0.02 (10)	0.794 ± 0.005 (13)	157.3 ± 0.6	L4.5 \pm 1.5 (13)	1680 ± 170 (13)	

* binary brown dwarf, see text

Reference: 1.) Nakajima et al., 1995; 2.) Leggett et al., 2002; 3.) Golimowski et al., 1998; 4.) Saumon et al., 2000; 5.) Potter et al., 2002; 6.) Gaidos, 1998; 7.) Gaidos, Henry & Henry, 2000; 8.) Fuhrmann, 2004; 9.) Goto et al., 2002; 10.) Valenti & Fischer, 2005; 11.) Lowrance et al., 2000; 12.) Zuckerman et al., 2001 13.) Liu et al., 2002

mini-survey of close BD companions using the mid-infrared imager VISIR at the VLT. Section 2 reviews the targets properties and describes our observations. Section 3 describes our data reduction and analysis process. Section 4 presents the results of our survey, i.e the photometry and the astrometry of the detected companions and the sensitivity limits obtained. Finally, Section 5 compares our results with the predictions of cool atmosphere models to discuss their applicability and limitations.

2. Target Properties and Observation

For our target selection, we have only considered the confirmed members of binary (or multiple) systems with known distances, as their primaries are well characterized in terms of metallicity and age. Then, only BD companions with expected mid-IR fluxes **stronger than 1 mJy** and separations larger than $0.5''$ were selected in order to fully adapt and exploit the sensitivity and spatial resolution of the mid-infrared imager VISIR at the VLT. We finally ended-up with a short list of four systems: GJ 229, HD 130948, HR 7329 and HR 7672. Their main characteristics are summarized in Table 1.

- GJ 229 B is the first unambiguous discovered BD (Nakajima et al., 1995). Later on, orbital motion was detected by Golimowski et al., 1998, who observed GJ 229 B at three epochs spread over approximately one year using HST’s Wide Field Planetary Camera 2 (WFPC2). Matthews et al., 1996 derived an effective temperature of ~ 900 K from the measured broadband spectrum of GJ 229 B, assuming a radius equal to that of Jupiter. The same effective temperature was obtained by Leggett et al., 1999 by comparing colours and luminosity to evolutionary models by Burrows et al., 1997. In general model spectra for GJ 229 B (Marley et al., 1996; Allard et al., 1996) reproduce the overall energy distribution fairly well and agree with $T_{eff} = 950$ K.
- HD 130948 BC is a binary brown dwarf companion detected by Potter et al., 2002. The separation between the two companions is $(0.134 \pm 0.005)''$ at $PA = (317 \pm 1)^\circ$. Both companions have the same spectral type (L4 \pm 1.) and effective temperatures ($T_{eff} = 1900 \pm 75$ K) (Goto et al., 2002).
- HR 7329 B is a BD companion detected by Lowrance et al., 2000 at a separation of $4''$ from the early-type star HR 7329 A, a member of the β Pictoris moving group (Zuckerman et al., 2001). Their optical spectrum points toward a spectral type M7/M8 and an effective

temperature of 2405 to 2770 K for this young substellar companion. Guenther et al., 2001 show evidence that the source is a co-moving companion.

- HR 7672 B, a common proper motion companion to the variable star HR 7672 A, was reported by Liu et al., 2002. They inferred an effective temperature of $T_{eff} = 1510 - 1850$ K for HR 7672 B and estimated an age of 1 - 3 Gyr for the system.

All targets have been observed using VISIR (Lagage et al., 2004) mounted at the UT3 (Melipal) with the filters PAH1 ($\lambda_{cen} = 8.59 \mu\text{m}$, $\Delta\lambda = 0.42 \mu\text{m}$), PAH2 ($\lambda_{cen} = 11.25 \mu\text{m}$, $\Delta\lambda = 0.59 \mu\text{m}$) and SIV ($\lambda_{cen} = 10.49 \mu\text{m}$, $\Delta\lambda = 0.16 \mu\text{m}$). A nominal pixelscale of $0.075''$ was used during all observations and standard chopping and nodding techniques, with a chop-throw amplitude of $6''$ and $8''$ for GJ 229, respectively, and a chopping frequency of 0.25 Hz were employed. The nodding direction was chosen parallel to the chopping direction and, consequently, with an equal nodding to chopping amplitude.

To assure that the primary as well as the companion are within the FoV during chopping and nodding the system was aligned horizontally on the detector. At the same time, this simplifies the reduction process, since the shift and add of the frames can be done using the brighter primary star. A summary of the observing log is given in Table 2., including the mean airmass during the observing run and the total integration time.

3. Data Analysis

3.1. Data Reduction

The reduction was done using self-written IDL routines for bad-pixel replacement as well as for the shift and add of the frames. Bad-pixel were replaced by the mean value of the surrounding pixels within a box of 9×9 pixel, before subtracting (A-B) nodding positions. In the following the relative shifts between the frames of one data-set were calculated via cross-correlation of the bright primary, before the frames were averaged. Since the VISIR detector was affected by randomly triggered stripes during part of the observations, a destriping technique developed by Pantin et al., 2007 was applied to the final, co-added images.

3.2. Aperture Photometry

Standard aperture photometry was used to determine the relative photometry of all detected BDs. Using IDL ATV routines,

Table 2. Observing Log.

Object	Filter	UT date dd/mm/yr	Airmass	DIMM ^a seeing ["]	humidity [%]	DIT [s]	NDIT	# of nods ^c	Int. Time ^d [s]	Calibrator
GJ 229	PAH1	08/01/06 ^b	1.109	0.91	17 - 50	0.016	123	12	2172.7	HD 26967, HD 75691
		10/02/06 ^b	1.195	0.79	23 - 55	0.016	123	18	3259.0	HD 41047, HD 75691
	PAH2	03/02/06 ^b	1.044	0.83	20 - 40	0.008	246	6	1086.3	HD 41047, HD 26967
		10/02/06	1.110	0.84	23 - 55	0.008	246	6	1086.3	HD 26967, HD 75691
	SIV	10/02/06	1.022	0.95	23 - 55	0.04	48	11	1943.0	HD 26967, HD 75691
HD 130948	PAH1	09-10/07/06	1.524	0.67	6 - 8	0.020	98	22	3967.0	HD 133774, HD 99167
	PAH2	11/07/06 ^b	1.541	0.91	7 - 10	0.010	197	22	3987.3	HD 149009
		04-05/08/06 ^b	1.734	0.71	7	0.010	197	11	1993.6	HD 149009, HD 145897
	SIV	03/08/06	1.627	0.86	5 - 8	0.040	48	11	1943.0	HD 145897
05/08/06		1.606	0.62	6 - 11	0.040	48	11	1943.0	HD 145897	
HR 7329	PAH1	07/06/06	1.182	1.05	4 - 12	0.020	98	22	3967.0	HD 178345
	PAH2	21/05/06	1.153	1.36	7 - 19	0.008	246	11	1991.6	HD 178345
	SIV	07/06/06	1.175	0.88	4 - 12	0.040	48	22	3886.1	HD 178345
HR 7672	PAH1	10/07/06 ^b	1.341	0.76	6 - 8	0.020	98	11	1983.5	HD 189695, HD 149009
		12/07/06 ^b	1.405	0.88	6 - 11	0.016	123	11	1991.6	HD 189695, HD 178345
	PAH2	10/07/06 ^b	1.385	0.81	6 - 8	0.010	197	11	1993.6	HD 189695, HD 220954
		13/07/06 ^b	1.693	0.78	5 - 8	0.010	197	11	1993.6	HD 198048, HD 217902
	SIV	13/07/06 ^b	1.356	0.82	5 - 8	0.040	48	15	2649.6	HD 178345, HD 198048

a.) in V band at 550 nm, b.) data showed stripes, c.) 23 chops per nod, d.) $t = \text{DIT} \times \text{NDIT} \times \# \text{ of chops} \times \# \text{ of nods} \times 4$

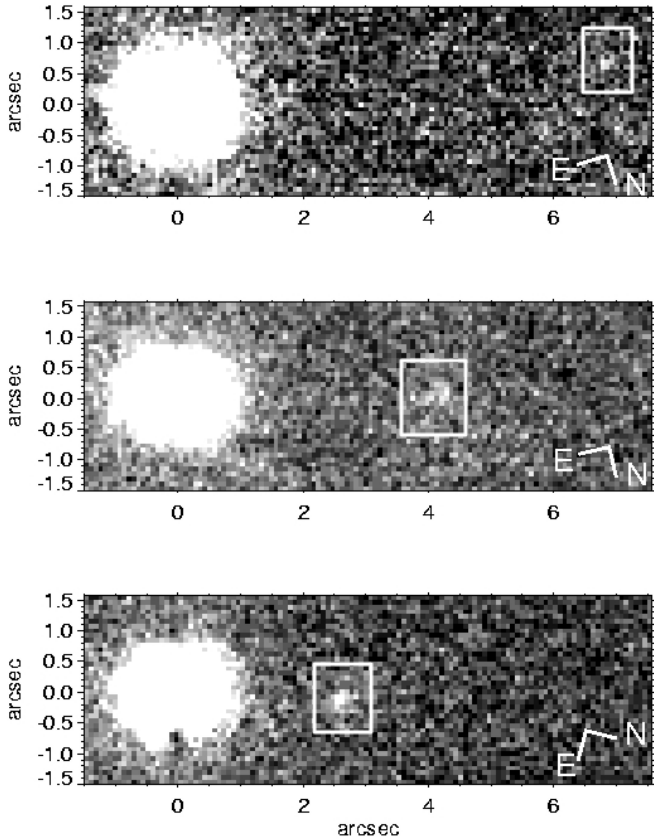


Fig. 1. VISIR detection images of GJ 299B at $\sim 6.8''$ (upper), HR 7329 at $\sim 4.3''$ (middle) and HD 130948 BC at $\sim 2.5''$ (bottom) at $8.6 \mu\text{m}$. To all images a σ filter with a box width of 5 pixel has been applied. Furthermore the N-E orientation of the data is over plotted in the lower right corner of the image.

curve-of-growth method was applied to the brown dwarf companions to obtain the apertures where the signal-to-noise ratio is maximised. In the following, those apertures were used for the primary as well as for the standard stars. Thus the count-rate to flux conversion factor was determined and relative photometry obtained. The variation of the count-rate to flux conversion factors with aperture radius was screened for at least 3 consecutive aperture radii between 4 and 7 pixels (corresponding to radii of $0.3''$ to $0.525''$). At $10 \mu\text{m}$ the VISIR diffraction limit is $\sim 0.3''$, the chosen aperture radii are of the order or twice the diffraction limit. To calibrate the flux values different standard stars,¹ observed before and after the targets, were used. The error bar estimation of the flux calibration is derived from the flux variations of the source measured in different apertures and from different standard stars. In case two independent measurements were taken an average of the measured flux is quoted in Table 4.

As already mentioned a destriping technique was applied to the final images to clean it from random stripes and therewith improve the image quality. To estimate the impact of the destriping on the photometry of the BD's, we performed the aperture photometry before and after the destriping process. In those cases in which the source is not located close to a stripe, no influence is notable. Whereas in the cases where the BD is close-by a stripe, a decrease in the measured count-rate, and consequently in flux, of the BD in the destriped images is perceivable. Nevertheless this effect is expected, since the stripes in the 'raw' images fall within the aperture radii and lead to an overestimation of the count-rate and therewith of the flux.

3.3. Detection limits

To estimate the detection limits as a function of angular separation two approaches were explored. The standard deviation of the intensities within a 1 pixel wide annulus at a given radius was determined as well as the standard deviation within a box of 5×5 pixels along a random radial direction. From the ob-

¹ Taken from the list of Cohen et al., 1999

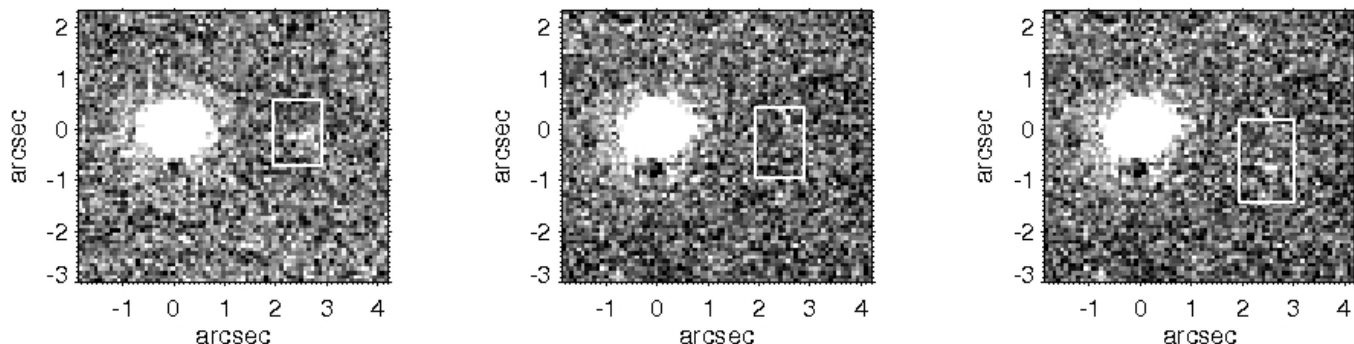


Fig. 2. VISIR images of HD 130948 in the SIV filter taken on the 5th of August (left) and on the 3rd of August (middle). The binary brown dwarf companion was detected in the data from the 5th of August and is marked by a box in the leftmost image. The flux was measured to be 5.7 ± 0.4 mJy. In the data set from the 3rd of August the companion was not detected. Its approximate location is at the same position as in the left image and also marked by a box. The right image shows the data from the 3rd of August, in which an artificial companion of 4 mJy had been placed. The artificial companion is located somewhat below the expected position of the real companion.

tained noise estimate the contrast with respect to the peak intensity of the primary was calculated (see, e.g., Figure 3). The detection limits delivered by both methods are in good agreement. Additionally, to further test the derived detection limits, artificial companions, with fluxes varying between 2 and 10 mJy, were placed within the data at separation between 1 and 5". The limiting fluxes of the re-detectable artificial companions match the previously derived detection limits. Up to a separation of $\sim 1.5''$ the detection limit is dominated by the photon noise of the central star and at larger separation the background noise from the atmosphere and the instrument limits our detections.

4. Results

Three of the four brown dwarfs were detected in PAH1, namely GJ 229 B, HR 7329 B and HD 130948 BC (see Figure 1); while only HD 130948 BC could be detected in SIV. Note that HD 130948 BC, a binary brown dwarf, was not resolved in our observations. In none of the filters HR 7672 B could be detected. While the resolution of VISIR is sufficient to separate the brown dwarf and the primary ($\sim 0.79''$ Liu et al., 2002; assuming orbital motion negligible), the data quality in PAH1 and SIV is low. The PSF of the primary is elongated, affecting the area in which the brown dwarf is expected, and thus adding noise.

In Table 3. the measured separations and position angles of the detected brown dwarfs are given. To obtain the separation as well as the position angle of the brown dwarfs relative to their primaries, the pixelscale and N-orientation provided in the image header were used. Golimowski et al., 1998, used the HST's Wide Field Planetary Camera 2 (WFPC2) to observe GJ 229 B at three epochs, which were spread over approximately one year. Orbital motion of GJ 229 B was detected and a relative change of separation of $(0.088 \pm 0.010)''$ per year was measured. In the last 10 years, from November 1996 to February 2006, the separation between GJ 229 A and B changed by $(0.894 \pm 0.05)''$, resulting in a average change of separation of $(0.097 \pm 0.005)''$ per year. For HD 130948 only a minor change of separation is observable. From February 2001 to July 2006 the separation between HD 130948 A and BC declined by $(0.09 \pm 0.05)''$. In case of HR 7329 no orbital motion was observable. Finally in Table 4. the obtained fluxes for the primary stars and the brown dwarfs, as

Table 3. Separations and position angles of the detected brown dwarfs.

Object	UT date	sep. [arcsec]	P.A. [°]
GJ 229	10/02/06	6.78 ± 0.05	168.4 ± 0.9
HD 130948	09/07/06	2.54 ± 0.05	103.9 ± 2.4
HR 7329	07/06/06	4.17 ± 0.11	167.2 ± 1.4

well as the upper limits for the non-detections are listed. In case of HD 130948 BC the flux measured in the data set from the 5th of August is quoted as well as the upper limit obtained on the 3rd of August. While the observations of HD 130948 BC in SIV have been carried out at two different epochs, on the 3rd and the 5th of August, the object was only detectable in the second data set, see Figure 2 with a measured flux of (5.7 ± 0.4) mJy. The non-detection of HD 130948 BC in the data set from the 3rd of August can not be explained by a discrepancy in the sensitivity limits, see Figure 3. Both data sets clearly reach the same sensitivity limit. Furthermore, simulations of artificial sources showed, that a companion with a flux of (4 ± 0.4) mJy (corresponding to a 5σ confidence level) would have been detected in both data sets. Hence, within ≈ 48 hours HD 130948 BC varied by at least (1.7 ± 0.6) mJy.

5. Discussion

5.1. Comparison with models

As a final step we compare our obtained photometry to the models by Allard et al., 2001 and Burrows et al., 2006. Using their theoretical spectra provided online² absolute model fluxes were calculated by integrating the theoretical spectrum over the VISIR filter bandpasses. The object radii R , which determine the absolute spectral flux calibration, were obtained from evolutionary calculations by Burrows et al., 1997. In Table 5. the calculated model fluxes are listed. Furthermore the age and effective temperature combinations for which the object

² <http://perso.ens-lyon.fr/france.allard/>
<http://zenith.as.arizona.edu/burrows/>

Table 5. Predicted mid-IR fluxes from different theoretical models. Values consistent within 3σ or with the given upper limit were marked in **boldface**.

Object	Reference	T_{eff} [K]	$\log g$ [cm/s ²]	[M/H]	age Myr	R/R _⊙	PAH1 [mJy]	SIV [mJy]	PAH2 [mJy]
GJ 229 B	Allard ^a	900	5.0	0.0	200	0.122	3.30	2.97	5.06
	Allard ^a	1000	5.0	0.0	200	0.122	4.67	4.55	6.68
	Allard ^a	1000	3.0	0.0	200	0.122	4.80	6.69	7.94
	Allard ^a	1000	3.0	0.0	30	0.133	5.70	7.95	9.44
	Burrows ^c	900	5.0	0.0	200	0.122	3.35	3.0	4.25
	Burrows ^c	900	5.0	-0.5	200	0.122	3.33	2.46	3.78
	Burrows ^c	1000	5.0	-0.5	200	0.122	4.25	3.44	4.77
	Burrows ^c	1000	5.0	-0.5	30	0.133	5.04	4.09	5.66
	Burrows ^c	1000	4.5	-0.5	30	0.133	5.14	4.99	6.05
	measured					3.2 ± 0.5	3.2 ¹	6.7 ¹	
HD 130948 BC	Allard ^b	1900	5.0	0.0	800	0.091	1.65	1.25	1.13
	Allard ^b	1900	5.0	0.0	300	0.102	2.07	1.57	1.42
	Allard ^b	1900	3.5	0.0	300	0.102	1.67	1.21	1.11
	Burrows ^d	1900	5.0	0.0	300	0.102	1.53	1.26	1.17
	Burrows ^d	1900	5.0	-0.5	300	0.102	1.49	1.25	1.16
		measured ²					1.9 ± 0.3	2.9 ± 0.3 ³	1.2 ¹
	measured ²						1.5 ¹		
HR 7329 B	Allard ^b	2400	4.0	0.0	12	0.193	1.06	0.91	0.79
	Allard ^b	2600	3.5	0.0	8	0.278	2.80	2.30	2.55
	Allard ^b	2600	3.5	0.0	12	0.229	1.90	1.56	1.73
	Allard ^b	2600	4.0	0.0	12	0.229	1.76	1.44	1.25
	Allard ^b	2800	4.0	0.0	12	0.265	2.84	2.20	1.91
		measured					3.2 ± 2.3	1.9 ¹	2.9 ¹

a.) AMES-cond models from Allard et al., 2001

b.) AMES-dusty models from Allard et al., 2001

c.) L & T cloud-free model from Burrows et al., 2006

d.) L & T model with clouds from Burrows et al., 2006

1.) upper limit, limiting background plus 3σ

2.) flux of one component assuming both L4 dwarfs contribute equally to the measured flux

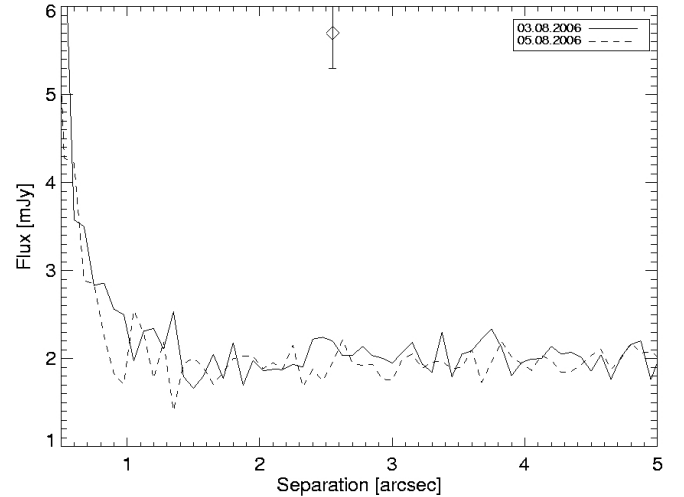
3.) only 05.08.2006

Table 4. VISIR Photometry of the primaries and brown dwarfs. In case of a non-detection upper limits are provided. The fluxes are quoted in mJy.

Object	PAH1	SIV	PAH2
GJ 229 A	1297. (47)	923. (33.)	793. (26.)
GJ 229 B	3.2 (0.5)	2. (0.3) ^a	4. ^a (0.9)
HD 130948 A	861. (5.)	605. (27.) ^b	478. (6.)
HD 130948 BC	3.8 (0.4)	5.7 (0.4) ^b	1.8 (0.2) ^a
HD 130948 A		553. (27.) ^c	
HD 130948 BC		2. (0.4) ^{a,c}	
HR 7329 A	524. (19.)	404. (3.)	386. (24.)
HR 7329 B	3.2 (2.3)	1.3 (0.2) ^a	2.3 (0.2) ^a
HR 7672 A	880. (36.)	554. (33.)	519. (14.)

a.) limiting background (1σ), b.) only 05.08.2006, c.) 03.08.2006

radius was determined are given. From Allard et al., 2001 we employed the AMES-cond and AMES-dusty models, representing the two extreme cases, in which either all dust has disappeared from the atmosphere (AMES-cond) or dust settling throughout the atmosphere is negligible (AMES-dusty). Following Allard et al., 2001 the AMES-dusty models should successfully describe dwarfs with effective temperatures greater than 1800 K, while the AMES-cond models are better suited to describe the atmospheres of dwarfs with $T_{eff} \leq 1300$ K.

**Fig. 3.** Comparison of the limiting background obtained from the two data sets of HD 130948 taken in the SIV filter. The overplotted point corresponds to the detection on the 5th of August, with a flux of 5.7 mJy.

GJ 229 B: Saumon et al., 2000, have used high-resolution infrared spectra to determine the metallicity, effective temperature and gravity of the T dwarf (see also Table 1.). While

using an age of 0.2 Gyr they derived an effective temperature of $950 \text{ K} \pm 80 \text{ K}$ and a gravity of $\log g = 5 \pm 0.5$. Later on, Leggett et al., 2002 compared observed low- and high-resolution spectra of GJ 229 A and GJ 229 B to theoretical spectra (AMES-models). Their best fit yields an $T_{\text{eff}} = 1000 \pm 100$ and a gravity of $\log g \leq 3.5$ for GJ 229 B as well as a metallicity of $[M/H] \approx -0.5$ and an age of ~ 30 Myr (range 16 - 45 Myr) for the system. While the metallicity is determined within the spectra fitting procedure, the age is derived by a comparison with evolutionary models and mainly constrained by the observed luminosity and the derived effective temperature of the A component. Using VISIR mid-IR photometry, absolute model predictions of both Allard et al., 2001 and Burrows et al., 2006 can then be tested for different combinations of T_{eff} , $[M/H]$ and gravity (when available, e.g. see Figure/4). From Table 5, we see that the PAH1, SIV and PAH2 photometry is consistent with model predictions for a $T_{\text{eff}} = 900 \text{ K}$, $\log g = 5.0$ and $[M/H] = 0$ companion. At solar metallicity, an effective temperature of $T_{\text{eff}} = 1000 \text{ K}$ can be excluded at more than 2 sigma. At subsolar $[M/H] = -0.5$ metallicity, low gravity ($\log g < 4.5$) values remain excluded for $T_{\text{eff}} = 1000 \text{ K}$. Therefore, excluding young ages predictions of Leggett et al., 2002, the VISIR photometry clearly favors the initial physical parameters proposed by Saumon et al., 2000 for solar and subsolar metallicities.

HD 130948 BC: As already mentioned HD 130948 BC is a binary brown dwarf consisting of two L4 dwarfs. In order to compare our observations to the model predictions we assumed that both brown dwarfs contribute equally to the measured fluxes, as simplest assumption. An unequal distribution of the measured flux on one of the two brown dwarfs would only increase the in the following described effect. The suggested effective temperature of $\sim 1900 \text{ K}$ places the binary in the regime of the AMES-dusty models. While the predicted PAH1 flux is in good agreement with our measurements, most models fail to reproduce the SIV flux detected on August 5 2006, but would be consistent with the non-detection of August 3 2007. Using the models provided by Burrows et al., 2006 we tested the influence of different metallicities ($[M/H]=0.0$ and $[M/H]=-0.5$) on the predicted fluxes. The change is marginally, only about 0.05 mJy.

5.2. HD 130948 BC: photometric variability

While analysing the SIV data obtained for HD 130948, we found that the binary companion was detectable in only one of the two data sets. A possible explanation of this result is an intrinsic variability around $10.5 \mu\text{m}$ of one or both of the L dwarfs in the binary. Variability at $10.5 \mu\text{m}$ could either be caused by ammonia (NH_3) or silicates. Since the NH_3 absorption features, which were first-time identified in the mid-infrared spectra taken with Spitzer/IRAS by Roellig et al., 2004, and Cushing et al., 2006, appear at roughly the L/T transition it is unlikely to be the cause of the observed variability. A more favourable explanation may be an inhomogeneous distribution of silicate clouds, which characterise the atmospheres of L dwarfs with effective temperatures of roughly 1400 - 2000 K (Burrows et al., 2001). Future VISIR observations of HD 130948 BC at $10.5 \mu\text{m}$ over different timescales should secure this photometric variability.

6. Summary

Using VISIR at the VLT we performed a mini-survey of brown dwarfs in binary systems. The four selected brown dwarfs were imaged in three narrow band filters at 8.6, 10.5 and $11.25 \mu\text{m}$.

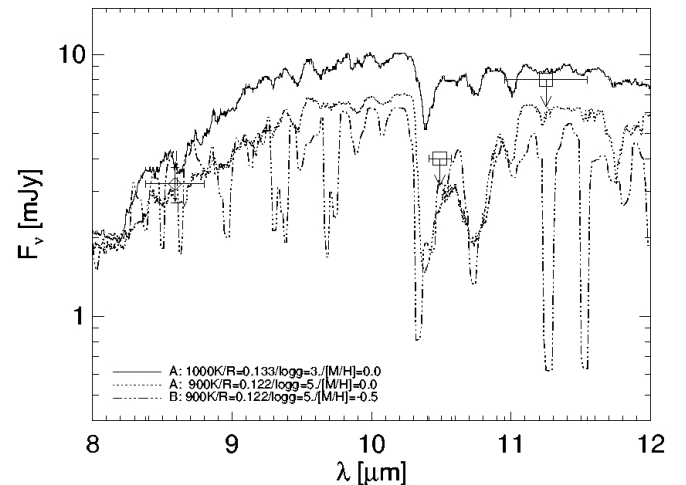


Fig. 4. GJ 229 B: Comparison of theoretical spectra from Allard et al., 2001 and Burrows et al., 2006 with the VISIR photometry.

At $8.6 \mu\text{m}$ three of the brown dwarfs were detected and photometry was obtained. None of the brown dwarfs was detected at $11.25 \mu\text{m}$ and only, HD 130948 BC, at $10.5 \mu\text{m}$. The observations of HD 130948 BC at $10.5 \mu\text{m}$ indicate a possible variation of one or both brown dwarfs of the binary.

To constrain the atmospheric properties of the brown dwarfs we compared the mid-infrared photometry to theoretical model spectra by Allard et al., 2001 and Burrows et al., 2006. The measured mid-infrared fluxes and upper limit, respectively, of GJ 229 B are consistent with the characteristic parameter obtained by Saumon et al., 2000 ($T_{\text{eff}} \sim 950 \text{ K}$, $\log g \sim 5$), while values of the effective temperature and gravity as suggested by Leggett et al., 2002 ($T_{\text{eff}} \sim 1000 \text{ K}$, $\log g \leq 3.5$) result in too high model fluxes. As for HD 130948 BC, the model fluxes for $T_{\text{eff}} \sim 1900 \text{ K}$, $\log g \leq 5$ fit the measurement at $8.6 \mu\text{m}$ and the upper limits obtained at $10.5 \mu\text{m}$ and $11.25 \mu\text{m}$. Nevertheless the models are not in agreement with the flux measured for the detection of HD 130948 BC at $10.5 \mu\text{m}$ during one observing epoch.

References

- Allard, F., Hauschildt, P.H., Alexander, D.R., et al. 2001, ApJ, 556, 357
 Allard, F., Hauschildt, P.H., Baraffe, I., & Chabrier, G. 1996, ApJ, 465, L123
 Burgasser, A.J., Kirkpatrick, J.D., Cutri, R.M., et al. 2000, ApJ, 531, L57
 Burrows, A., Sudarsky, D., Hubeny, I. 2006, ApJ, 640, 1063
 Burrows, A., Hubbard, W.B., Lunine, J.I., et al., 2001, RvMP, 73, 719
 Burrows, A., Marley, M., Hubbard, W.B., et al. 1997, ApJ, 491, 856
 Chen, B., Asai, R., Figueras, F., et al. 1997, A&A, 318, 29
 Cohen, M., Walker, R.G., Carter, B., et al. 1999, AJ, 117, 1864
 Cushing, M.C., Roellig, Th.L., Marley, M.S., et al. 2006, ApJ, 648, 614
 Cutri, R.M., Skrutskie, M.F., van Dyk, S., et al. 2003, 2MASS All-Sky Catalog of Point Sources
 Epchtein, N., de Batz, B., Capolani, L., et al. 1997, The Messenger, 87, 27
 Fuhrmann, K. 2004, AN, 325, No.1, 3
 Gaidos, E.J. 1998, PASP, 110, 1259
 Gaidos, E.J., Henry, G.W., & Henry, S.M. 2000, AJ, 120, 1006
 Golimowski, D.A.; Burrows, C.J.; Kulkarni, S.R., et al. 1998, AJ, 115, 2579
 Goto, M., Kobayashi, N., Terada, H. 2002, ApJ, 567, L59
 Guenther, E.W., Neuhäuser, R., Huélamo, N., et al. 2001, A&A, 365, 514
 Lagage, P.O., Pel, J.W., Authier, M. et al. 2004, The Messenger, 117, 12
 Leggett, S.K., Saumon, D., Marley, M.S., et al. 2007, ApJ, 655, 1079
 Leggett, S.K., Hauschildt, P.H., Allard, F., et al. 2002 MNRAS, 332, 78

- Leggett, S.K., Toomey, D.W., Geballe, T.R., et al. 1999, *ApJ*, 517, L139
- Liu, M.C., Fischer, D.A., Graham, J.R., et al. 2002, *ApJ*, 571, 519
- Lowrance, P.J., Schneider, G., Kirkpatrick, J.D., et al. 2000, *ApJ*, 541, 390
- Mainzer, A.K., Roellig, Th.L., Saumon, D., et al. 2007, [astro-ph/0701398]
- Marley, M.S., Saumon, D., Guillot, T., et al. 1996, *Science*, 272, 1919
- Matthews, K., Nakajima, T., Kulkarni, S.R., et al. 1996, *AJ*, 112, 1678
- Nakajima, T., Oppenheimer, B.R., Kulkarni, S.R., et al. 1995, *Nature*, 378, 463
- Pantin, E., Vanzi, L. & Weilenman, U. 2007, to appear in the proceedings of the ESO Instrument Calibration Workshop 2007
- Potter, D., Martin, E.L., Cushing, M.C., et al. 2002, *ApJ*, 567, L133
- Roellig, T.L., van Cleve, J.E., Sloan, G.C., et al. 2004, *ApJS*, 154, 418
- Saumon, D., Geballe, T.R., Leggett, S.K., et al. 2000, *ApJ*, 541, 374
- Saumon, D., Marley, M.S., Cushing, M.C., et al. 2006, *ApJ*, 647, 552
- Sonderblom, D.R., Mayor, M. 1993, *AJ*, 105, 226
- Sterzik, M.F., Pantin, E., Hartung, M., et al. 2005, *A&A*, 436, L39
- Stoughton, C., Lupton, R.H., Bernardi, M., et al. 2002, *AJ*, 123, 485
- Valenti, J.A. & Fischer, D.A. 2005, *ApJS*, 159, 141
- Zuckerman, B., Song, I., Bessell, M.S. et al. 2001, *ApJ*, 562, L87